

Machine learning-based optimization design of bistable curved shell structures with variable thickness

Junbang Liu ^{a, b, &}, Jinke Chang ^{c, &}, Jizhou Yu^{a, b}, Wenhua Zhang ^{a, b, *}, Shiqing Huang ^{a, b, *}

^aMOE key Lab of Disaster Forecast and Control in Engineering Jinan University Guangzhou 510632, PR China

^bSchool of Mechanics and Construction Engineering Jinan University, Guangzhou 510630, PR China

^cDivision of Surgery & Interventional Science, University College London, London NW3 2PF, UK

ARTICLE INFO

Keywords:

Curved shell

Bistable

Backward snapping force

Structural optimization

Machine learning

ABSTRACT

The mechanical performance of curved shell structures is difficult to predict due to their complex geometric nonlinearity. There have been many efforts to improve the mechanical property of curved shell structures by designing the thickness distributions. However, due to the nonlinear characteristics of variable-thickness shells, it is impossible to exhaust all possible structural forms through experimental and theoretical approaches. In this paper, we report a new machine learning (ML)-based approach to design and optimize bistable curved shell structures. The ML model is used to establish the underlying mapping relationship between structural parameters and specific performance. Nonlinear shell structures are efficiently and accurately designed and optimized with optimal backward snapping forces (B). The results demonstrate an effective approach for the design and optimization of curved shell structures and provide a valuable reference for future study of nonlinear structures. Moreover, this approach presents an efficient means of designing advanced metamaterials. The modular design of meta-atoms based on ML has the potential to construct metamaterials with specific properties and functionalities, which will lead to extensive applications in different fields.

7

1. Introduction

8 Curved shell structures have been widely used in various engineering fields, such as aerospace, vehicle, pressure
9 vessel, instruments and apparatuses, et al [1]. Owing to their multi-stability, curved shell structures can also be applied as
10 typical unit elements to construct some novel architected metamaterials for energy trapping[2, 3]. It is scarcely possible to
11 fabricate these architected metamaterials by traditional manufacturing technologies in the past, and it is very difficult to
12 predict their non-linear mechanical behaviours theoretically. The extensive implementation of mechanical metamaterials
13 in engineering may face significant limitations. Advancements in manufacturing technologies such as 3D printing [4-
14 6]offer potential solutions to these challenges. Even mechanical metamaterials with complex geometries can be more
15 readily fabricated [7], and their mechanical properties can be further altered by adjusting the printing parameters [8].
16 Meanwhile, machine learning, combined with finite element analysis (FEA), provides a feasible method for predicting and
17 optimizing the mechanical properties of architected metamaterials [9]. Rapidly developing industries bring up new
18 demands to architected metamaterials, such as to be lightweight [10], negative Poisson's ratio [11], negative stiffness [12],
19 energy absorption [13]. Therefore, it becomes essential to propose an appropriate reverse optimization design method for
20 the bistable properties of curved shell structures based on ML.
21

22 Compared with curved beams, curved shell structures have some similar or even better mechanical properties [14], such
23 as negative stiffness [15, 16], multi-stability [17-19], and excellent energy absorption [20-23]. Over the past few decades,

[&]These authors contributed equally to this work and should be considered co-first authors

* Corresponding author.

E-mail address: zwhdwy@hnu.edu.cn (W. H Zhang); thuangsq@jnu.edu.cn (S.Q. Huang).

1 significant efforts have been devoted to the approximate theoretical analysis, numerical simulations, and experimental
2 investigations of the mechanical properties of shell structures[24-26], among them, Civalek et al. have made great
3 contributions to solving the motion control differential equations of shell structures, using a series of numerical analysis
4 methods including Generalized Differential Quadrature (GDQ) [27], Discrete Singular Convolution (DSC) [28, 29],
5 DSC- Differential Quadrature (DQ) coupling method [30] and higher-order shear-normal deformation theory and analytical
6 approach to the static analysis, etc. Due to the geometric complexity of the shell structures and the limitations of the
7 manufacturing process, so far, most of the researches have only been focused on the curved shell structures with regular
8 shape and uniform thickness [31-34]. Previously, researchers have investigated the impact of diverse shell structure
9 geometries, thicknesses, and material distributions on the mechanical characteristics [35-37]. Stegmann et al.
10 [36]introduced a material optimization method called Discrete Material Optimization (DMO) to maximize the structural
11 stiffness of the shell. Shimoda et al. [37] proposed a new numerical shape optimization method for shell structures, and the
12 obtained shape is an excellent shell load-bearing structure that can be applied to automobiles, airplanes and ships.
13 Optimizing the thickness distribution of a bistable shell structure entails achieving maximum utilization of materials in
14 each of its constituent parts, while ensuring equal mass. This is a crucial factor that holds significant importance in the field
15 of energy absorption [38, 39]. The reverse optimization design of curved shell structures, especially with a variable
16 thickness distribution, is still a big challenge as the design space is too large to be exhaustive. A variety of optimization
17 algorithms have been put forward to solve this reverse problem, such as ant colony algorithm [40], particle swarm algorithm
18 [41], level set method[42], density method [43] and evolutionary approach [44], etc. The ant colony algorithm and particle
19 swarm algorithm in topology optimization combine topology optimization and bionic concepts [45, 46]. The level set
20 method simplifies complex boundary shapes and flexibly tunes complex topological changes [42]. Although these
21 techniques achieve great success not only in mechanical design problems but also in other physical disciplines such as
22 fluids and acoustics [47, 48], there are still many challenges including the high computational expense, the limited
23 application range of compliance minimization problems, and the difficulty to apply more geometric and physical constraints
24 [49].

25 Since ML was first coined by Arthur Samuel in the 1950s [50], it has achieved great success in image recognition [51],
26 speech recognition [52], medical prediction [53], and recommendation engines [54], and so on. It has been recognized that
27 the core capability of ML is to detect and construct the complex internal correlations of input and output variables from a
28 large-scale dataset. Therefore, it is credible that the non-linear relationship between the geometric parameters of a structure
29 and its mechanical performance can also be obtained through ML in principle on the basis of building the dataset through
30 finite element analysis [55]. Based on the established correlation, the corresponding optimization of the shape of the
31 structure can be easily carried out for various optimization objectives.

32 Researchers have employed ML to investigate complex optimization and prediction problems in the field of mechanics,
33 such as metamaterials, auxetic structures and fluid mechanics [56-60]. For example, Wu et al. [56] used genetic ML
34 algorithms based on Bayesian framework to investigate the relationship between structural parameters and performances,
35 and optimized the meta-atom with enhanced performances. Hanakata et al. [57] used the convolutional neural networks
36 (CNN) to establish the nonlinear relationship between the cutting position and the mechanical properties of graphene
37 kirigami, and developed an optimal stretchable kirigami design. Qiu et al. [14] investigated the bistable properties of curved
38 beams, based on which Liu et al. [58] further proposed an inverse structural design of curved beam with optimized
39 properties based on ML. The research of Liu et al. gives inspiration to this paper about bistable properties of the curved
40 shell. To design auxetic structures with specific Poisson's ratio, Wang et al. [59] developed a back propagation neural
41 network (BPNN)-genetic algorithm (GA) model to reversely forecast specified Poisson's ratio structural parameters.
42 Mosavi et al. [60] also utilized ML in analysis of fluids, which accurately predicted the macroscopic parameters based on

1 adaptive-network-based fuzzy inference system (ANFIS). Many studies have demonstrated that ML can be a promising
2 approach for dealing with nonlinear problems in mechanics, and have been successfully used for optimization of simple
3 structures like beams and columns [61, 62]. We believe that the problem of complex structural optimization for curved
4 shells with nonlinear properties can also be tackled using ML.

5 In this research, we present an inversed design approach using fully connected neural networks and an optimized
6 shape generator. Curved shell structures are designed and optimized to obtain a maximum backward snapping force (B).
7 We firstly investigate the general mechanical properties of curved shell structures, conduct FEA on curved shells, and
8 propose a structural variation mode and the feasibility verification of this variation mode. Then, the ML structure and
9 optimization methods are described. Based on the ML model, reverse optimization is conducted with multiple self-learning
10 loops to determine the optimal structure to the targeted performance. Finally, we demonstrate the effect of the ML model
11 after training with datasets of FEA and obtain the curved shell shape with the larger absolute value of the backward snapping
12 force, and compare the FEA results of the predicted shape with the results predicted by the ML model. Several studies have
13 employed new ML approaches for directing the shape optimization of nonlinear structures [63-65]. However, to the best
14 of our knowledge, the reverse optimization of shell structures utilizing ML techniques remains an unexplored research area.
15 Compared with the mainstream structural design methods [38, 45, 46], the method presented in this paper constitutes a
16 significant advance in the design objectives of dynamic problems and nonlinear optimization, with a notable reduction in
17 computational costs. The study also introduces a novel thickness distribution redistribution approach for shell structures to
18 obtain the maximum backward snapping force (B). The ML-based optimization method has strong transferability that can
19 be applied in the parametric design of most mechanical structures. The optimized curved shell unit cell could also be further
20 expanded for the development of metamaterials.

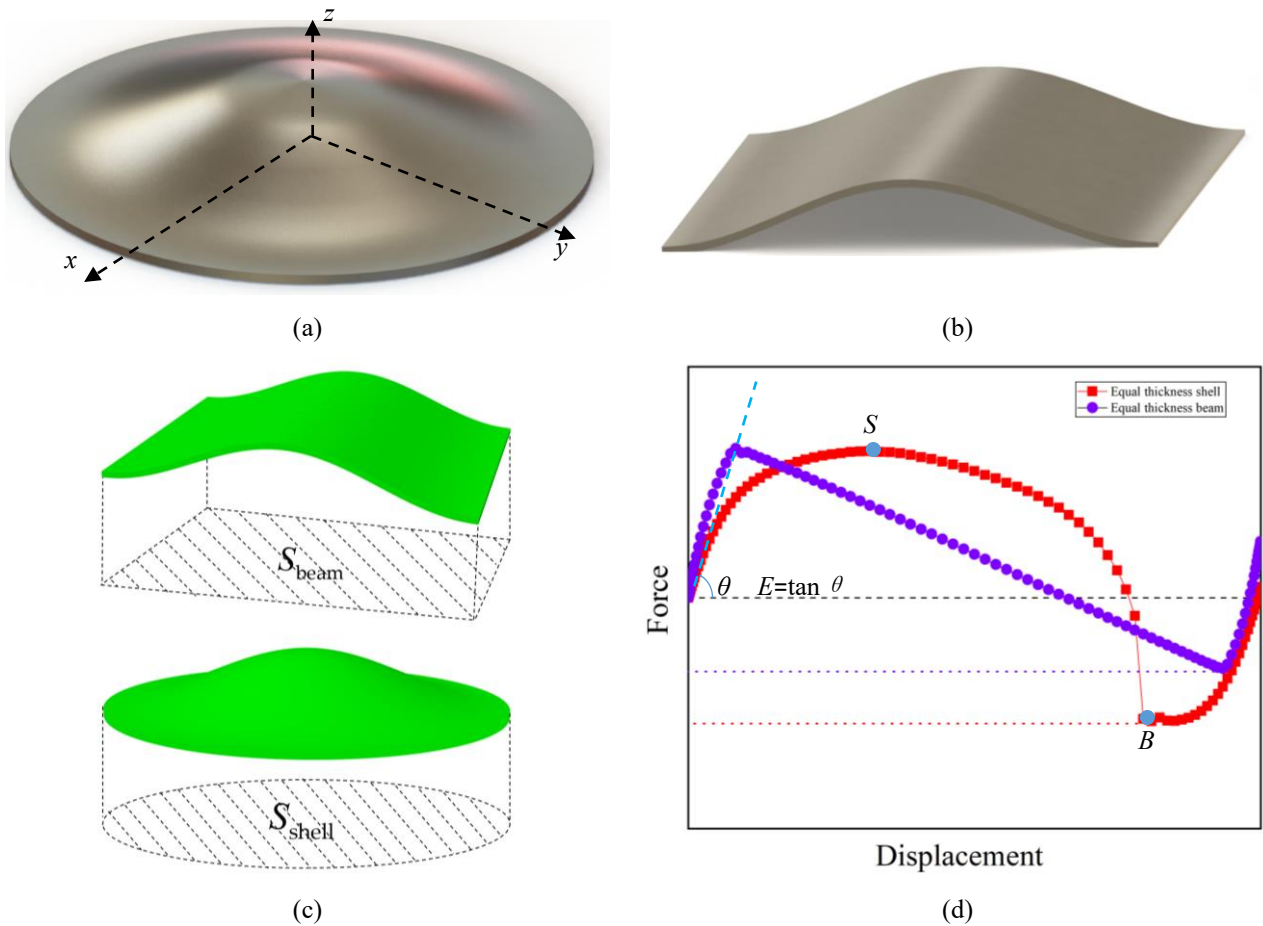
21 **2. FEA modeling for bistability of curved shell structures**

22 Curved shell structures may have bistability when their geometric parameters are selected appropriately, which is
23 similar to pre-shaped curve beams. When a curved shell is in a bistable state, it will not automatically return to the initial
24 state after removing the external load, but store energy until the system is subjected to enough reverse disturbances to return
25 to the initial state. Therefore, the bistable curved shells can be applied to construct architected metamaterials for energy
26 trapping.

27 A rotationally symmetric curved shell can be obtained by rotating a pre-shaped curved beam 360 degrees about its
28 axis of symmetry, as shown in Fig. 1(a). Referring to the cylindrical coordinate system with the origin located on the center
29 of the projected circle, the initial shape of the curved shell can be expressed as follows.

$$30 \quad w(x) = \frac{h}{2} \left[1 + \cos \frac{2\pi r}{L} \right], \quad (1)$$

31 where L is the span and h is the initial apex height of the curved shell with thickness $t(r)$. A vertical force is subjected to
32 the apex of the shell as shown in Fig. 1(a) and the displacement boundary condition around the outermost circle is assumed
33 to be clamped.



1 Fig. 1 Comparison of mechanical properties between beams and shells of equal thickness under the same mass;(a)&(b) solid model
 2 diagrams of equal-thickness curved shells and equal-thickness curved beams (c) the FE model of the equal-mass curved beam and curved
 3 shell with the same vertical project, $S_{beam} = S_{shell}$, (d) the results of force-displacement curve.

4 Through finite element analysis, the typical load-displacement curve can be obtained as shown in Fig. 1(d). Similar
 5 to a curved beam, the highly nonlinear load-displacement curve has three stages, from which three mechanical properties
 6 of the curved shell can be extracted: stiffness (E), forward snapping force (S) and backward snapping force (B). Wherein,
 7 backward snapping force (B) is the most important sign of whether the curved shell is bistable. If $B < 0$, the curved shell is
 8 bistable. When the absolute value of the backward snapping force (B) is larger, it means that the structure needs to absorb
 9 more energy after entering the second steady state to make the modal step, and the structure is more stable in the second
 10 steady state. Therefore, it is considered to find a structure with a larger absolute value of the backward snapping force to
 11 maximize its stability in the second steady state. So, the goal now is to use the method provided in this paper to find a
 12 suitable structural form in an infinite design space to make the absolute value of the backward snapping force as large as
 13 possible. As shown in Fig. 1(c-d), after FE calculating the equal-mass curved beam and curved shell with the same vertical
 14 project area, it is obvious that the shell better than the beam in the mechanical property of the backward snapping force.

15 Qiu et al. deduced that in order to achieve bistability, a curved beam with equal thickness t must satisfy the condition
 16 of the ratio $Q = h_0/t \leq 2.31$ between the arch height and the beam thickness, it is also proposed that changing the thickness
 17 distribution of the beam can also optimize the bistable characteristics of the beam to a certain extent. Inspired by this, we
 18 optimizes the target mechanical properties by changing the thickness distribution of the curved shell as shown in Fig. 2(a-
 19 b).Fig. 2(c) is sectional view of FE model of a variable-thickness shell. Fig. 2(d) is the force-displacement curve calculated
 20 from three curved shells with the same mass but different thickness distributions. It shows that there are three different

1 cases of the backward snapping force (B), $B_1 > 0$, $B_2 = 0$ or $B_3 < 0$, which shows that by changing the thickness distribution
 2 of the shell to reconstruct the structure, the magnitude of the backward snapping force can be completely controlled. When
 3 the backward snapping force (B) is less than 0, it means that the curved shell structure can have bistable properties. When
 4 the absolute value of the backward snapping force (B) is larger, it means that the structure needs to absorb more energy
 5 after entering the second steady state to make the modal step, and the structure is more stable in the second steady state.
 6 Therefore, it is considered to find a structure with a larger absolute value of the backward snapping force to maximize its
 7 stability in the second steady state. So, the goal now is to use the method provided in this paper to find a suitable structural
 8 form in an infinite design space to make the absolute value of the backward snapping force as large as possible.

9 In FE calculations, considering the need for subsequent large-scale data operations to establish a database, FE software
 10 and Python language must have good interaction functions, and select ABAQUS for FE simulation calculation. The
 11 establishment and calculation process of the FE model of the curved shell is as follows: (1) the symmetrical curved shell
 12 model is established by establishing the script input analytical formula Eq.(1), $L = 60\text{mm}$, $h = 8\text{mm}$, and thickness is $t =$
 13 1mm ; (2) the curved shell model is divided into FE meshes, and the S4R shell element is selected for the FE discretization
 14 of the geometric model, and the edge length of the FE mesh is set to 0.5mm ; (3) define the material properties, the research
 15 object in this paper is 316L stainless steel, which is an elastic-plastic material. Its constitutive relationship is the true stress-
 16 strain curve obtained from the test. The material parameters used are shown in Table 1; (4) the boundary conditions are set
 17 as follows: the edge of the curved shell is set as a fixed constraint. In order to prevent the asymmetric mode of the curved
 18 shell, a displacement load of $2h$ is applied at the vertex of the circular shell, and there is only a translational degree of
 19 freedom in the vertical position; (5) this analysis involves the buckling behavior of the structure. The structure must
 20 release the strain energy to maintain equilibrium. We use a dynamic approach to the buckling response, a quasi-static
 21 analysis.

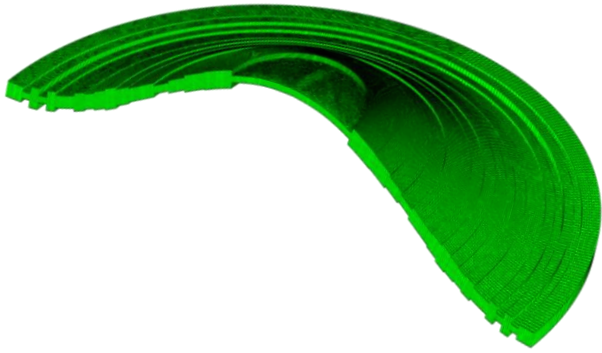
22 Table 1 Material parameters

Material	Elastic Modulus	Density	Poisson's ratio
316L stainless steel	206GPa	7.98g/cm ³	0.3

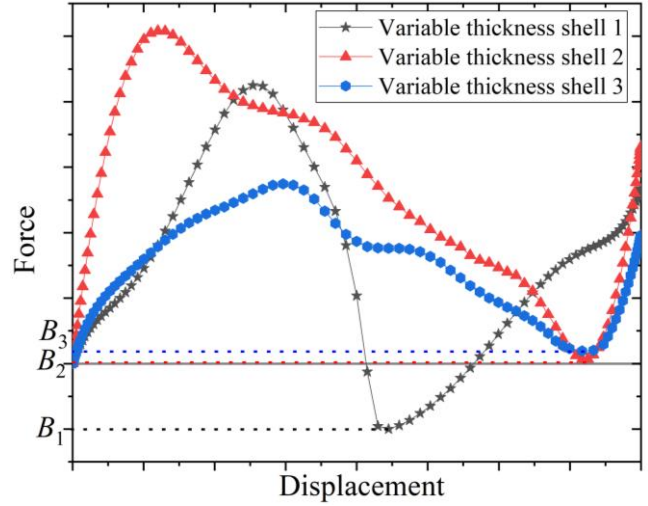
23 The FE modeling of the above curved shell is completed in the FE software ABAQUS, the analysis step is defined,
 24 the large deformation is opened, the field variables and history variables are selected to output the results, and the model
 25 is calculated and analyzed.

26





(c)



(d)

1 Fig. 2 Curved shell solid model diagram. (a) Axonometric view of solid model of varying thickness curved shell; (b) Sectional view of
 2 solid model of varying thickness curved shell; (c) Sectional view of the FE model of varying thickness curved shell; (d) Force-
 3 displacement curves of several types of variable-thickness curved shells under the same material and equal mass, backward snapping
 4 force ($B_i, i = 1, 2, 3$).

5 3. Machine learning model

6 3.1 Re-entrant structure

7 Fig. 3(a) shows the geometric configuration of a curved shell with variable thickness, which involves 20 control
 8 parameters that control the relative size of the 20-segment annular shell thickness respectively. According to several trial
 9 calculation results in Fig. 2(d), it is proved that the curved shell under the same material and quality can change its
 10 mechanical properties by changing its thickness distribution, including the backward snapping force of the research object
 11 in this paper. Therefore, the backward snapping force of re-entrant structure is determined as a function of variables $t_i, [i=1,$
 12 $2, 3, \dots, 19, 20]$, this function will be determined by the ML model constructed below.

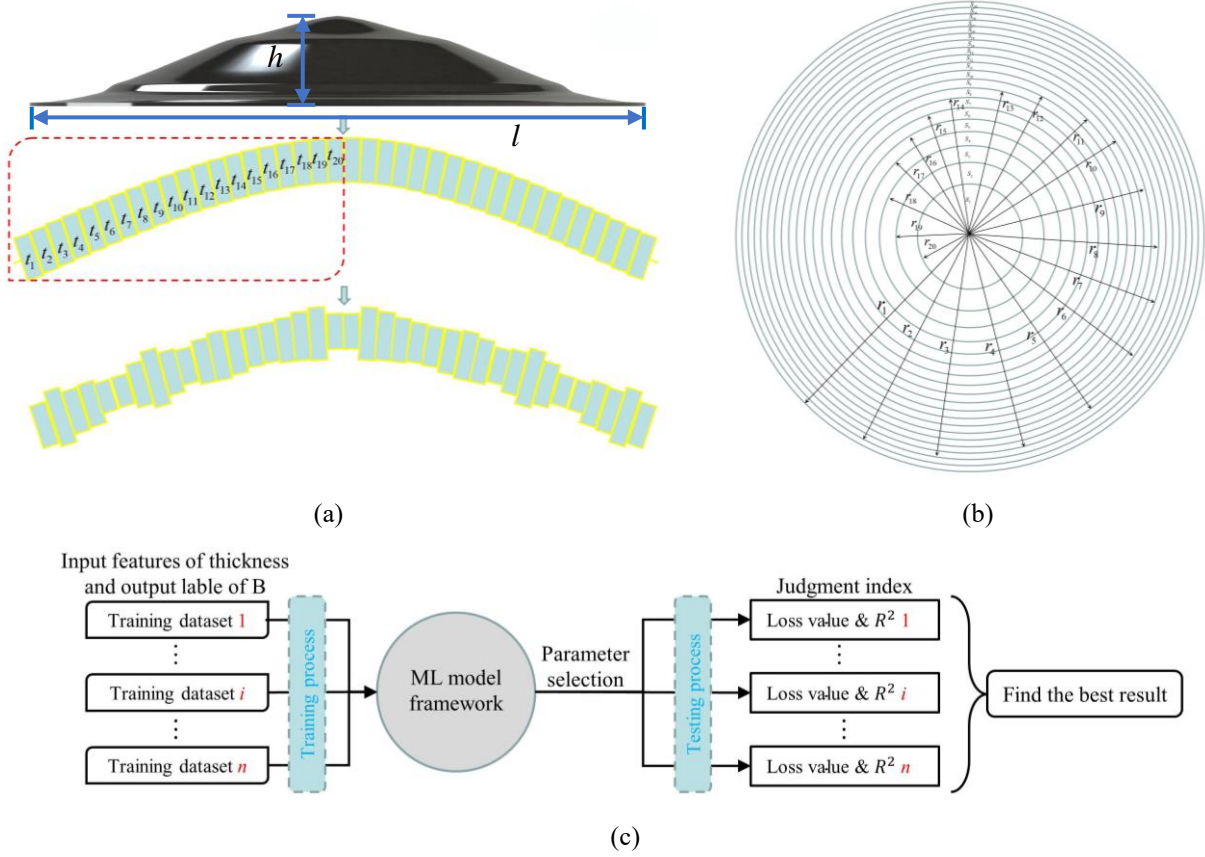
13 3.2 Machine learning model construction

14 In this section, a ML model is constructed for cyclic optimization of the thickness distribution of curved shells. The
 15 construction of the ML model mainly consists of two processes: training and testing. The purpose of the training process
 16 is to obtain a one-to-one mapping approximation function f that describes the relationship of the input variable x to get $y =$
 17 $f(x)$. By training the dataset, a ML model is obtained, which can be regarded as $D = \{(x_i, y_i) | i = 1 \rightarrow n\}$.

18 3.2.1 Dataset construction

19 A database is established including input features and output labels. The geometric parameters of the curved shell
 20 analytical formula Eq.(1) used for optimization are: $l = 60, h = 8$. By changing the constant $t_i, i \in [1, 2, 3, \dots, 18, 19, 20]$.
 21 As Fig. 3(a) shows, an array with 20 numbers representing the relative thicknesses of the 20 sections. All relative
 22 thicknesses are randomly selected in the array $t_i \in [1.0, 1.1, 1.2, 1.3, 1.4, 1.5, 1.6, 1.7, 1.8, 1.9, 2.0]$, and also satisfy the
 23 constraints $t_{\max}/t_{\min} \leq 2$, which means that for each variable thickness curved shell its thickest part of the ring will not

- 1 exceed 2 times the thinnest part of the ring. This constraint can be changed by adjusting the array to suit individual needs.
- 2 Therefore, the training process of building a ML model is to build the mapping relationship $B = f(t_1, t_2, t_3, \dots, t_{18}, t_{19}, t_{20})$
- 3 between $(t_1, t_2, t_3, \dots, t_{18}, t_{19}, t_{20})$ and the backward snapping force (B).



4 Fig. 3 Building the training datasets. (a) Structure of the equal-thickness shell is re-entrant to the process of changing the thickness of
5 the irregular shell, where t is the relative thickness of each section; envelope treatment is used after the final optimization to avoid stress
6 concentration; (b) Top view of curved shell. The radius r of each part is determined, which ensures that $S_1 = S_2 = \dots = S_{20}$. (c) Selection
7 process of ML models after training using training datasets of different sizes. The i -th dataset has 10^4 more data than the $(i-1)$ -th dataset.
8 When the loss value and R^2 value obtained after training with the n -th dataset are not greater than those after training with the $(n-1)$ -th
9 dataset, $n \times 10^4$ training data is selected as the dataset.

10 The input data used to train the ML model is an array of relative thicknesses. Note that the relative thickness array
11 must be converted to the actual thickness array in finite element (FE) simulations. The output data is backward snapping
12 force (B) from FE simulation results.

13 To ensure all curved shell models have the same quality as the original equal thickness curved shell, and to enhance
14 the reliability of the final optimization results, the following transformations are needed. First solve Eq. (4), the goal is to
15 ensure that the area of each ring is consistent as shown Fig. 3(b), which is $S_1 = S_2 = \dots = S_{20}$,

$$16 \quad \begin{cases} 2r_{m+1}^2 - r_{m+2}^2 - r_m^2 = 0 \\ 2r_{20}^2 - r_{19}^2 = 0 \end{cases}, m = [1, 2, 3 \dots 17, 18], \quad (2)$$

17 we know $r_1 = 30$, so can get the width of each ring on the curved shell. Then the mass can be normalized by Eq. (5) to
18 realize the conversion of relative thickness and real thickness,

$$19 \quad t_i^o = t_i / \sum_{i=1}^{20} t_i \times 20, \quad (3)$$

1 where t_i^o is the real thickness array, t_i is the relative thickness array.

2 Each curved shell has 20 sections while each of which has 11 possible relative thicknesses. There are 11^{20} possible
 3 combinations. This is already a design space close to infinity. In such a complex and highly nonlinear situation, ML
 4 undoubtedly provides the most likely way to find the optimal structure. We randomly generate several thickness arrays of
 5 variable-thickness shells, which are used as input features of thickness and convert the actual thickness. The mechanical
 6 response is calculated in the FE software as output data which are the datasets used to train the ML model. Since we do not
 7 know the number of datasets required to achieve the optimal effect of the ML model, we use the method of constructing
 8 multiple dataset, and use the loss function mean square error (MSE) indicator [66] and the coefficient of determination R^2
 9 indicator [66] to determine the effect of the model:

$$10 \quad R^2(y, \hat{y}) = 1 - \frac{\sum_{i=1}^m (y_i - \hat{y}_i)^2}{\sum_{i=1}^m (y_i - \bar{y})^2}, \quad (4)$$

$$11 \quad MSE(y, \hat{y}) = \frac{1}{m} \sum_{i=1}^m (y_i - \hat{y}_i)^2, \quad (5)$$

12 Nine datasets are constructed here, the first datasets include 10^4 data, and then each datasets increase 10^4 data more
 13 than the previous datasets until the last datasets includes 9×10^4 data. There are a total of nine training datasets of different
 14 sizes. In order to test the prediction accuracy of the ML model after each training, nine additional datasets [$n \times 10^3$ ($n = 1, 2,$
 15 $3, \dots, 8, 9$)] which are completely independent of the training set were created using FE software, called test datasets. Each
 16 test datasets is 10% of the corresponding training dataset, it is used to detect whether the model has overfitting[67] and test
 17 the prediction accuracy of the final ML model, and select the ML model with the best effect. Remove the above nine
 18 datasets, three datasets with numbers of 100, 1000, and 5000 were created at the same time for trial training of the ML
 19 model. The whole process is shown in Fig. 3(c).

20 3.2.2 Machine learning model parameter

21 After obtaining the datasets, the second step is to determine the ML model algorithm and parameters, and use the
 22 datasets obtained in the first step to train the model. Keras [66] is currently the most widely used machine- learning
 23 framework. This paper considers using the Keras framework for building ML models. First determine the type of model,
 24 considering the highly nonlinear relationship between input features of thickness and output labels of backward snapping
 25 force, the goal is to build a regression-type fitting model, and the neural network sequential model is preferred. As the most
 26 widely used artificial neural network (ANN) algorithm at present, BPNN proposed by Rumelhart et al. in 1986 [68] is a
 27 multi-layer feedforward network trained by error back-propagation algorithm in Fig. 4(a). The basic flow of the
 28 backpropagation algorithm in Fig. 4(b). The composition and operation mechanism of a single neuron in a neural network
 29 in Fig. 4(c). When the input information x is passed to a certain hidden layer node, assuming the hidden layer output value
 30 is y , the neuron node will adjust the resulting approximation through a nonlinear activation function [69] to capture the
 31 nonlinear relationship between the input variable and the intermediate approximation, this intermediate approximation is
 32 y ,

$$33 \quad y = \sigma \left[\left(\sum_{i=1}^n \omega_i x_i \right) + b \right], i = 1 \rightarrow n, \quad (6)$$

34 where ω_i is the weight connecting the input layer x_i and the hidden layer unit. b is the correlation bias. σ is a continuously

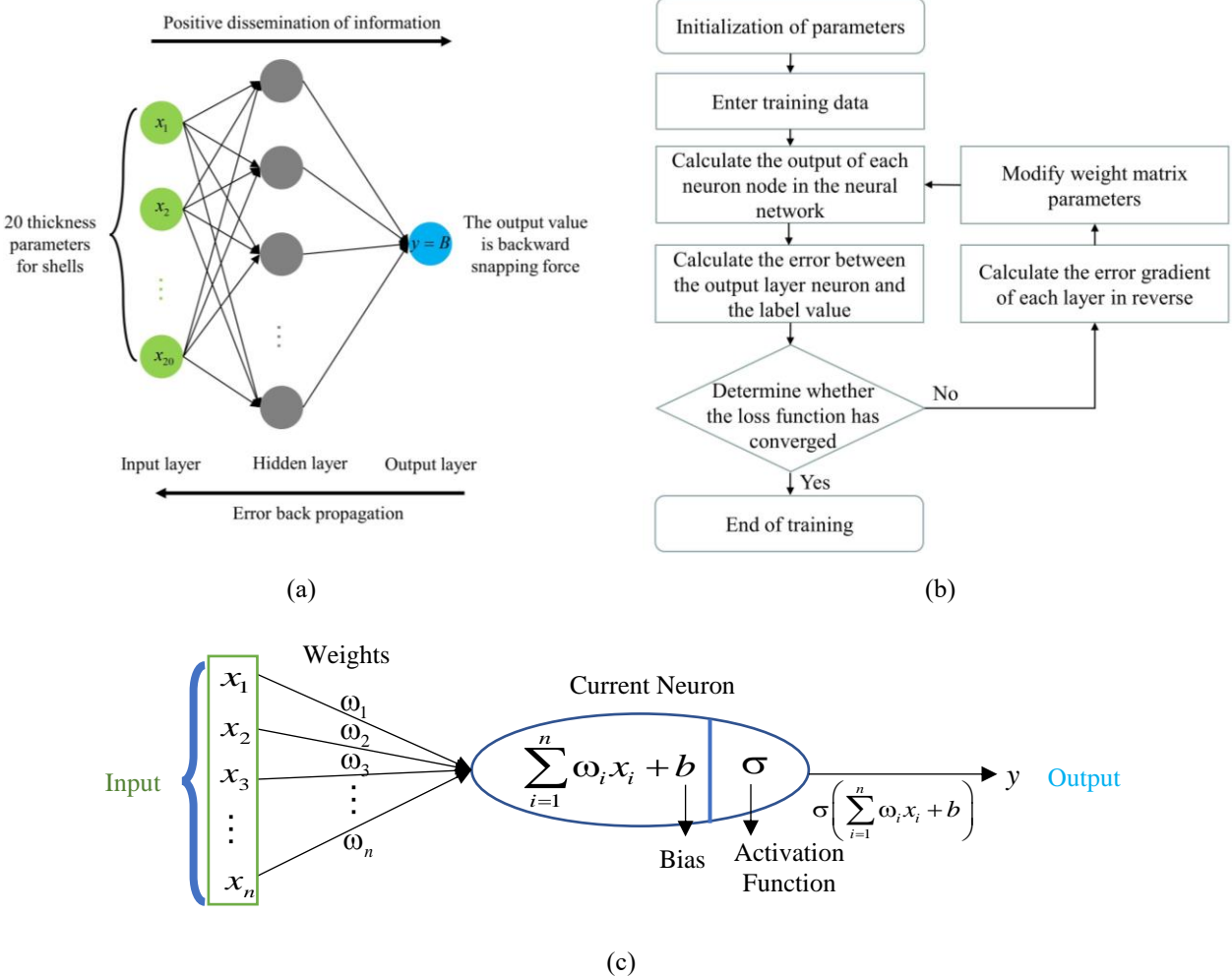
1 differentiable nonlinear activation function. In a neural network, the input layer and output layer are fixed, the number of
 2 hidden layers is tentative, and the type of optimizer and activation function needs to be determined. The choice of the loss
 3 function is also critical, which is related to the accuracy of the entire backpropagation process [66].

4 Before training, perform a data cleaning on the data set to identify some outliers, eliminate possible adverse effects
 5 on the results, make the distribution of all backward snapping forces according to the bar graph Fig. 5(a), we can see that
 6 they are in line with the Gaussian normal distribution. Consider using 3σ methods in Fig. 5(b). The probability that the
 7 value is distributed in $(\mu - 3\sigma, \mu + 3\sigma)$ is 99.73%, and the values beyond this range is an outlier.

8 After the data cleaning is completed, the data is preprocessed to remove a few finite element models that cannot be
 9 converged. Considering that the order of magnitude difference between features and labels is too large, the data samples
 10 are standardized according to the following formula:

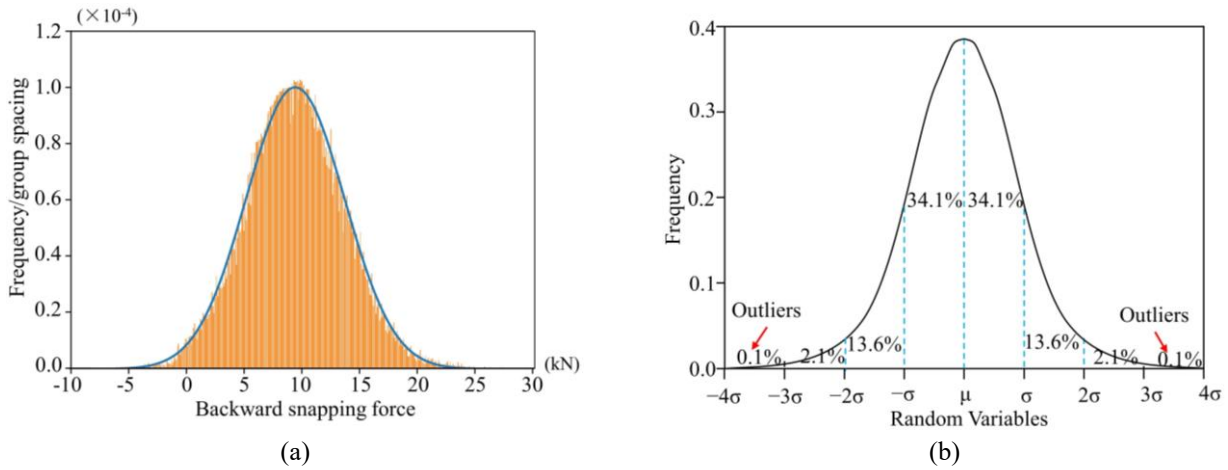
11
$$X^* = \frac{X - \mu}{\sigma}, \tag{7}$$

12 where μ is the mean of all sample data, σ is the standard deviation of all sample data. This step of processing can speed up
 13 gradient descent to find the optimal solution, improve accuracy, and prevent model gradient explosion.



14 Fig. 4 BPNN structure and principal diagram. (a) Diagram of the overall algorithm structure of BPNN. For the structure proposed in this
 15 paper, it includes 20 nodes in the input layer, several hidden layer nodes, and 1 output layer node. (b) Diagram of the basic flow of the
 16 BPNN algorithm. (c) The basic composition of a single neuron, including input, weight, bias function, activation function, output, and
 17 other elements.

1 The framework of ML was constructed as shown in Fig. 4(a). For the hidden layer, we need to determine the number
 2 of layers and nodes. It is generally believed that increasing the number of hidden layers can reduce the network error and
 3 improve the accuracy, but it also complicates the network, thereby increasing the training time of the network and even the
 4 tendency of overfitting. In order to know whether there is an overfitting problem in the ML model, it is necessary to use
 5 the previously constructed testing datasets set to verify the ML model. Methods to prevent overfitting include, but are not
 6 limited to, L2 regularization, adding Dropout layers [70, 71] to simplify neural network models and constantly tuning
 7 hyper-parameters. Generally, designing a neural network gives priority to a three-layer network (one hidden layer). In
 8 theory, one hidden layer can already fit any nonlinear mapping. Therefore, in this model, under the comprehensive
 9 consideration of training time cost and accuracy, one hidden layer is preferentially selected, and the parameters are adjusted
 10 by changing the number of hidden layer nodes. The number of nodes was selected from [120, 240, 360, 480, 600, 720, 840,
 11 960, 1020, 1200]. The ML model was trained with the training dataset described above. During the training process, we
 12 evaluated how well the model is performing and determine that this model provides satisfactory results by the loss function
 13 MSE error and coefficient of determination R^2 of the training and test sets.



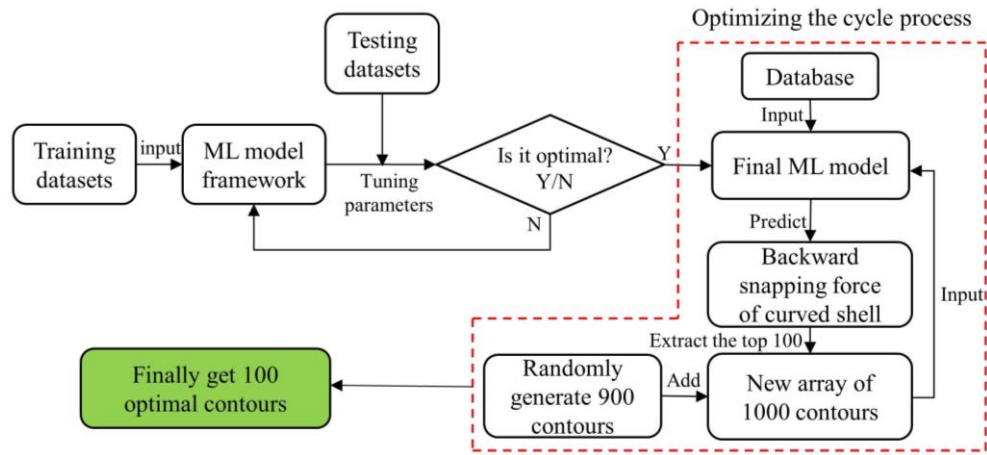
14 Fig. 5 Data cleaning process. (a) The size distribution of the backward snapping force in FEA results of the training data. The blue curve
 15 is the fitted curve according to the vertices of the histogram. (b) Standard Gaussian normal distribution plot. Data beyond 3σ are
 16 considered outliers and should be cleaned.

17 The choice of activation function is also important. According to the characteristics of the data, we choose among the
 18 four activation function of Sigmoid, Tanh, ReLU and PReLU [69]. The optimizer we choose in Adam and SGD [66]. The
 19 loss function we considers the mean squared error (MSE) and the mean absolute error (MAE) [66]. To sum up, there are
 20 160 ($10 \times 4 \times 2 \times 2$) parameter combinations, and we filter the best through grid search. Following all the above steps, an ML
 21 model was built specifically for predicting the mechanical properties of curved shells with different thickness distributions.

22 3.3 Self-learning optimization loop for machine learning models

23 The self-learning optimization loop process was used to train and test the ML model for targeted performance. We
 24 followed the general optimization procedure proposed by Gu et al. [72] The optimization flow chart is shown in Fig. 6.
 25 First, we use the ML model to predict all the datasets, sort all the predicted results, extract the top 100 results and the
 26 corresponding contours, and then use these 100 contours in the next loop plus 900 randomly generated contours, a total of
 27 1000 contours are re-predicted by the ML model. This is a cyclic optimization process. It is possible that some of the 900
 28 randomly generated contour samples will perform mechanically better than the top 100 passed in the previous cycle. After
 29 each cycle, there is a probability to find some better contour. Through multiple optimization iterations, curved shells with

1 better mechanical properties can be obtained.



2
3 Fig. 6 The position of the self-learning optimization loop process of the ML model in the whole process of this article.

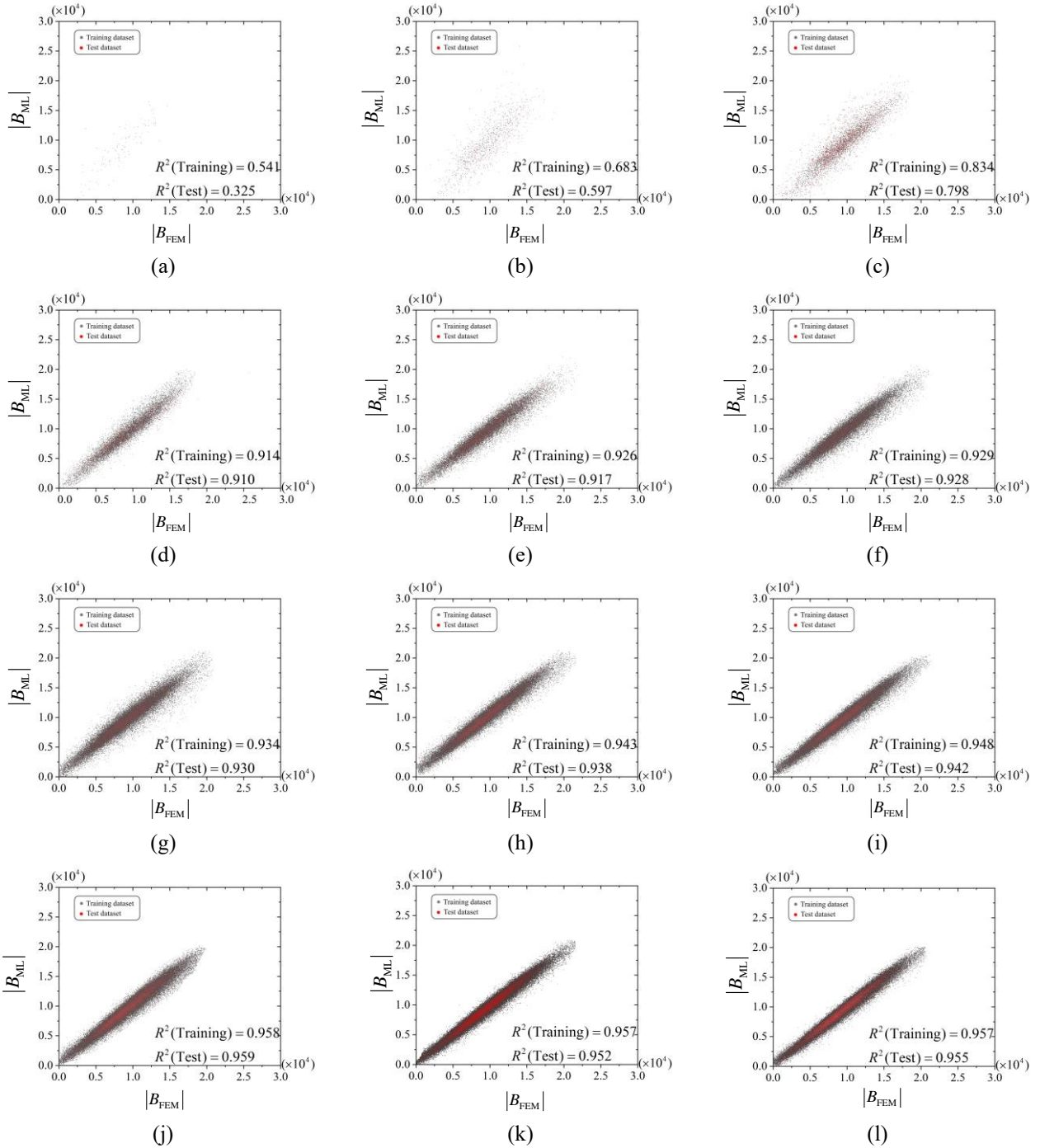
4 4. Comparison and discussion of results

5 The calculation time of each numerical simulation is about 20 seconds on the Intel Xeon E5-1650 central processing
6 unit (CPU), and there are a total of 450,000s FE calculations in a total of nine datasets. In this work, we optimize the
7 backward snapping force (B) in the force-displacement curve of the curved shell structure, and the goal is to find its largest
8 absolute value as much as possible. The results show that the mechanical properties of the curved shell can be changed by
9 changing the thickness distribution, and the target structure can be found effectively.

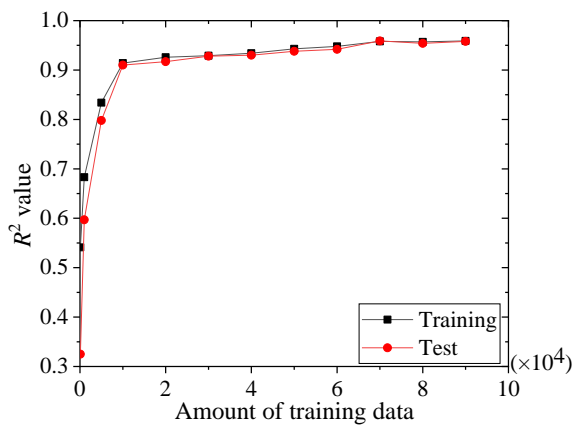
10 For ML models, we find the best parameters with the most accurate predictive models by grid search. The final selected
11 ML model parameters are: the number of neurons in a single hidden layer is 960, the activation functions used in the hidden
12 layer and the output layer are the PReLU function and the Linear function respectively, the loss function is MSE, the
13 optimizer is Adam, and the initial learning rate is 0.001. To prevent overfitting, set the L2 regularization parameter to 0.001
14 and the Dropout layer parameter to 0.3. During error backpropagation, Epoch is set to 200 and Batchsize is set to 128. The
15 training time for obtaining a complete ML model is about 1h, and the prediction of a mechanical performance result is
16 about 10^{-4} seconds, which is about 10^6 times faster than the FE simulation.

17 Fig. 7 shows that the different effects of our ML model trained with 12 different numbers of datasets. In order to verify
18 the model fitting degree after each training, the ML prediction value and FEM result of the test datasets are output in the
19 form of coordinates, and the loss function curve and the R^2 value are used to judge whether the ML model achieves the
20 desired effect. The loss of the testing dataset and the loss of the training dataset have converged and remain similar,
21 indicating that there is no overfitting, and the coefficient of determination R^2 of the training set and the test set are both
22 above 0.95, indicating that the ML model can accurately predict mechanical performance. In Fig. 7, the points of the
23 training datasets and testing datasets are basically distributed around the line $y = x$, which proves that the fitting degree of
24 the model is relatively good, and it has a high prediction accuracy. From the variation trend of R^2 in Fig. 8(a), it can be seen
25 that the fitting effect of the constructed 12 datasets when the amount of data exceeds 10^4 has achieved good results, and
26 the effect has been improved according to the increase of the training dataset, but when the number of training sets increases
27 to after 7×10^4 , the effect of improving the ML model is negligible, and there is even a possibility of reducing performance.
28 Therefore, the selection of the amount of data also needs to be confirmed by experiments.

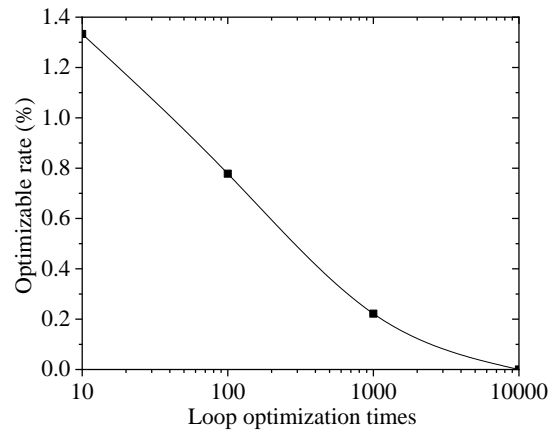
29



1 Fig. 7 Training effect on twelve datasets of different numbers. (a–c) are the effects of ML model by 100, 1000, 5000 training data. (d–l)
2 are the effects of the ML model trained by the $[n \times 10^4, n = (1, 2, 3, 4, 5, 6, 7, 8, 9)]$ training data. The black dots represent the training
3 dataset. The red dots represent the test dataset. The abscissa represents the FE simulation of the posterior occlusal force. The ordinate
4 represents the predicted value output by the ML model according to the thickness distribution.

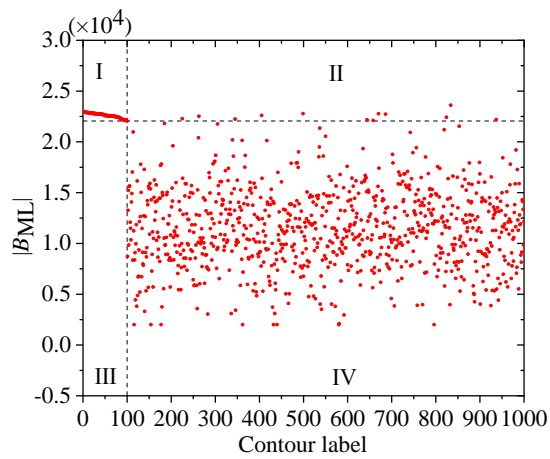


(a)

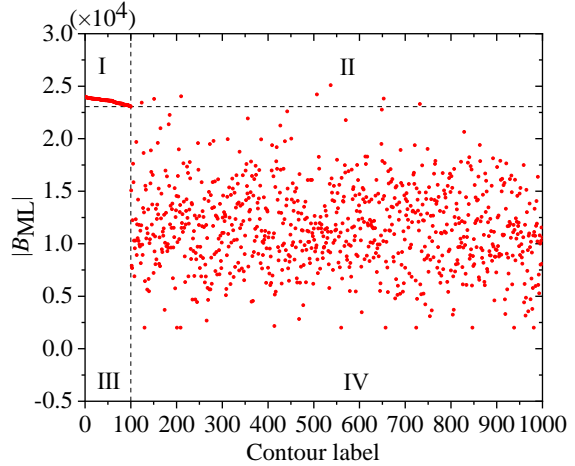


(b)

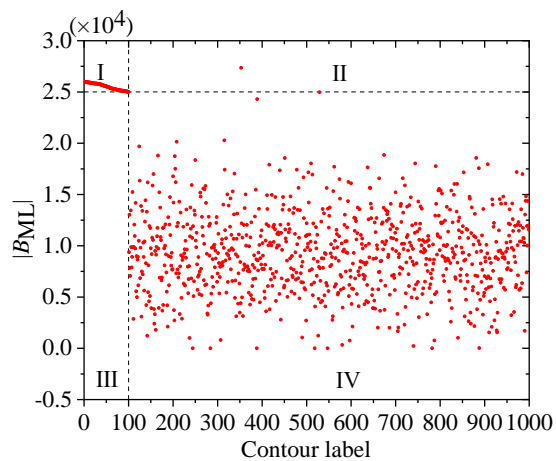
1 Fig. 8 (a) The R^2 values corresponding to the ML models trained by the twelve datasets. (b) The change in the optimizable rate over the
 2 entire design interval.



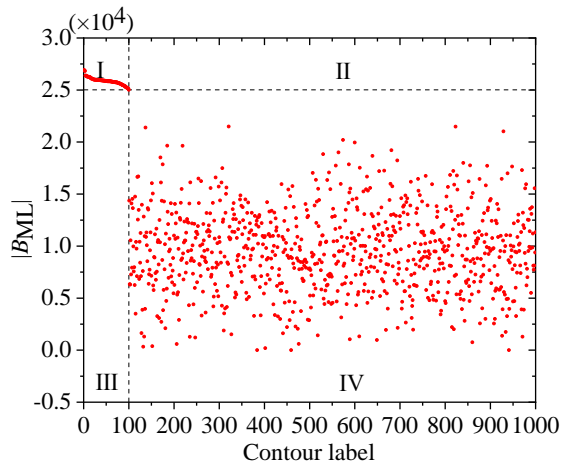
(a)



(b)



(c)

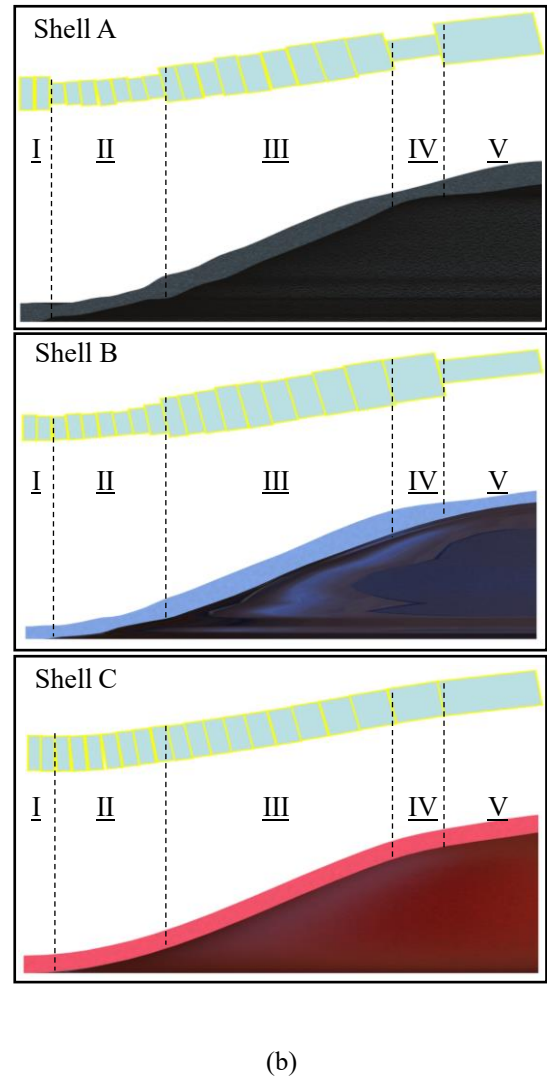
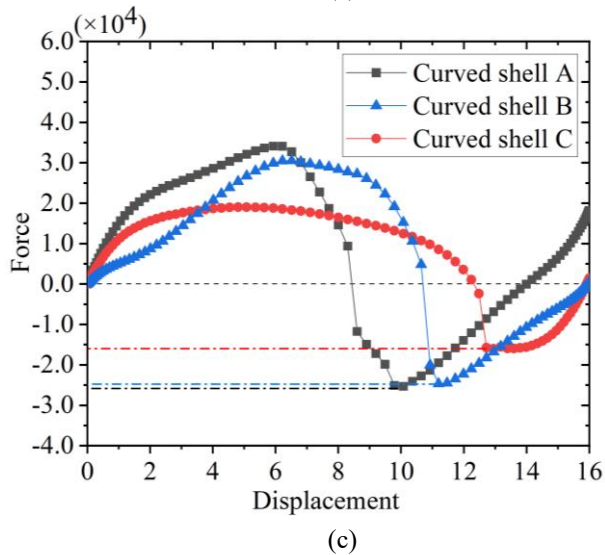
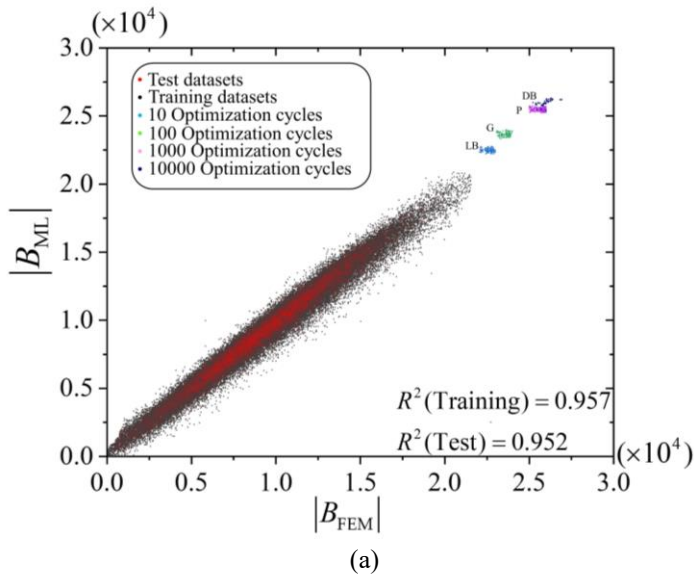


(d)

3 Fig. 9 The case of excellent contour generation after multiple self-learning optimization loops. (a) After 10 optimization cycles, the top
 4 100 excellent solutions in the previous cycle and the 900 random contours generated during this cycle. (b) After 10^2 optimization cycles,
 5 the top 100 excellent solutions in the previous cycle and the 900 random contours generated during this cycle. (c) After 10^3 optimization

1 cycles, the top 100 excellent solutions in the previous cycle and the 900 random contours generated during this cycle. (d) After 10^4
2 optimization cycles, the top 100 excellent solutions in the previous cycle and the 900 random contours generated during this cycle.

3 It can be seen in Fig. 9(a) that after 10 cycles of optimization, the mechanical properties of 12 of the 900 random
4 contours generated are better than the first 100 excellent contours passed down from the previous cycle, the number of
5 points in the II region that can be discharged into the I region in the next cycle is 12, and this number becomes 7, 2, and 0
6 respectively in Fig. 9(b–d). Define the optimizable rate in this loop optimization process as the number of points in area
7 II/total number of points in areas II and IV, and the change trend diagram of the optimal rate can be obtained as shown in
8 Fig. 8(b). With the continuous increase of the number of loop iterations, the optimization rate becomes lower and lower.
9 After loop optimization 10^4 times, the optimization rate is basically close to 0. It is in the process of continuous cyclic
10 optimization that the screening is realized, so that the top 100 excellent contours are continuously updated and iterated. It
11 can be seen from Fig. 9(d) that there are no points in the II region. The existence of chance is not ruled out, but the overall
12 trend can show that with the continuous increase of the number of self-learning loop optimization, the optimization space
13 is gradually compressed to converge to 0. It can be considered now that the thickness distribution of the curved shell with
14 better performance for the optimization target in the entire design space is found.



1 Fig. 10 Structural optimization results and FE validation tests. (a) The distribution of the excellent solutions after cycle optimization.
 2 The light blue (LB) points are the distribution of 100 excellent solutions after 10 cycles optimizations. The green (G) points are the
 3 distribution of the 100 excellent solutions after the 10^2 cycles optimization. The pink (P) points are the distribution of the 100 excellent
 4 solutions after the 10^3 cycles optimization. The dark blue (DB) points are the distribution of the 100 excellent solutions after the 10^4
 5 cycles optimization. (b) The thickness distribution of the excellent variable-thickness shells A, B and the constant-thickness shell C
 6 obtained after optimization, and the half-section profile after enveloping processing. (c) The force-displacement curve obtained by the
 7 FE simulation of A, B, C.

8 Fig. 10 (a) shows that there is still relatively obvious optimization space between 10 cycles, 10^2 cycles, and 10^3 cycles.
 9 The optimization obtained after 10^3 cycles already partially overlaps with the results obtained after 10^4 cycles, and it can
 10 be considered that the self-learning cycle optimization process is close to convergence. Considering the calculation cost
 11 and calculation accuracy, the contour of the curved shell after 10^4 cycles of optimization is extracted as the mechanical
 12 shape corresponding to the mechanical properties we need to optimize, that is, the thickness distribution.

13 Among the optimal contours, two possible shapes are mainly generated as shown in Fig. 10 (b). According to the
 14 optimized curved shell section shape, we can roughly divide the variable-thickness curved shell section into five parts I, II,

1 III, IV, and V as shown in Fig. 10 (b). In part I, there are two possibilities: thicker (A) and thinner (B). The thickness
2 distribution of the three parts II, III and IV is regular thin, thick, and thin. In part V, there are two possibilities of thicker
3 (A) and thinner (B). For the curved shell, the bending energy increases monotonically during the shell deflection, while the
4 compression energy first increases and then decreases during snap-through. It is the dominance of the change of the
5 compression energy over the bending energy that gives bistability. Thus, a shell shape that minimizes the change in bending
6 energy relative to the change in compression energy during shell deflection can help enhance the bistability. Since from the
7 shell section, the two boundary positions and the vicinity of the central position are the positions with the maximum bending
8 stress, the thickness of these three positions is reduced, and the effect of bending on the structure is significantly reduced.
9 This is an energy interpretation that fits the profile of the second type of optimized structure. For the first type of optimized
10 structural profile generated, it may be that the two ends will generate a large stress concentration during the deformation
11 process, which evolves into a relatively thick thickness at the constraints at both ends.

12 From Fig. 10 (c), after 10^4 cycles of optimization, the backward snapping force performance of the variable-thickness
13 circular shell structure is improved by about 1.7 times compared with that of the equal thickness curved shell. Therefore,
14 it is proved that the absolute value of the occlusal force after the round shell structure can be significantly improved by
15 changing the thickness distribution, and an excellent solution corresponding to the optimization objective is found through
16 the self-learning optimization loop method proposed in this paper.

17 The above curved shell structure is obtained after using the ML model to perform 10^4 optimization cycles, and the
18 optimization rate is close to 0. It is not ruled out that there are other better designs, but the profile design found here can
19 correctly guide the design how to achieve the structural form in which the absolute value of the backward snapping force
20 of the bistable curved shell is maximized.

21 5. Conclusions

22 In this paper, the main work includes using FE software to interact with python to perform large-scale calculations to
23 obtain the datasets about input features of thickness and output labels of backward snapping force, build ML models, and
24 propose a complete flow of structural self-learning optimization loops based on ML models. A variable-thickness curved
25 shell model was calculated by FEA about 20s, but it only takes 10^{-4} s to predict using the ML model, which is about 10^6
26 times faster than the FE calculation. After training and testing the ML model with different numbers of datasets, the R^2
27 value of the final selected ML model reached more than 0.95, which fully met the prediction accuracy requirements. The
28 backward snapping force of curved shells can be accurately predicted by inputting the thickness distribution, which solves
29 the bistable problem of variable thickness curved shells that cannot be accurately calculated in theory. And through the
30 proposed structure self-learning optimization loop method, the half-section thickness distribution patterns of two types of
31 optimized curved shell profiles are rough [thin, thin, thick, thin, thin] and [thick, thin, thick, thin, thick]. Under the condition
32 of equal quality, the backward snapping force of the curved shell after optimization with variable thickness is 2.6×10^4 N,
33 which is increased to 170% of the equal thickness (the backward snapping force is 1.6×10^4 N). The purposeful structure
34 optimization is realized. The self-learning optimization method based on ML model has great practical significance for the
35 design of a series of nonlinear structures. This method can be used for most structural optimization work in which the
36 structural parameter-property relationship is nonlinear. Our research shows that ML models are effective tools for nonlinear
37 structural design and optimization, and can have wider application space in interdisciplinary fields.

1 6. Acknowledgements

2 The authors thankfully acknowledge the financial support from the National Natural Science Foundation of China
3 (NO. 12102143), Young Talent Support Project of Guangzhou Association for Science and Technology, and the Fellowship
4 of China Postdoctoral Science Foundation (2022M711333). Thanks to Guangquan Wan for his support in ML.

5 References

- 6 1. Degenhardt, R., et al., *Future structural stability design for composite space and airframe structures*. Thin-Walled
7 Structures, 2014. **81**: p. 29-38.
- 8 2. Evans, K., *The design of doubly curved sandwich panels with honeycomb cores*. Composite structures, 1991. **17**(2):
9 p. 95-111.
- 10 3. Cheng, L., et al., *The twisting of dome-like metamaterial from brittle to ductile*. Advanced Science, 2021. **8**(13):
11 p. 2002701.
- 12 4. DebRoy, T., et al., *Additive manufacturing of metallic components - Process, structure and properties*. Progress
13 in Materials Science, 2018. **92**: p. 112-224.
- 14 5. Herzog, D., et al., *Additive manufacturing of metals*. Acta Materialia, 2016. **117**: p. 371-392.
- 15 6. Lewandowski, J.J. and M. Seifi, *Metal Additive Manufacturing: A Review of Mechanical Properties*, in *Annual*
16 *Review of Materials Research, Vol 46*, D.R. Clarke, Editor. 2016. p. 151-186.
- 17 7. Askari, M., et al., *Additive manufacturing of metamaterials: A review*. Additive Manufacturing, 2020. **36**: p.
18 101562.
- 19 8. Palaniyappan, S., et al. *Development and optimization of lattice structure on the walnut shell reinforced PLA*
20 *composite for the tensile strength and dimensional error properties*. in *Structures*. 2022. Elsevier.
- 21 9. Wang, Y., et al., *Inverse design of shell-based mechanical metamaterial with customized loading curves based on*
22 *machine learning and genetic algorithm*. Computer Methods in Applied Mechanics and Engineering, 2022. **401**:
23 p. 115571.
- 24 10. Sui, N., et al., *A lightweight yet sound-proof honeycomb acoustic metamaterial*. Applied Physics Letters, 2015.
25 **106**(17): p. 171905.
- 26 11. Lei, M., et al., *3D printing of auxetic metamaterials with digitally reprogrammable shape*. ACS applied materials
27 & interfaces, 2019. **11**(25): p. 22768-22776.
- 28 12. Tan, X., et al., *Real-time tunable negative stiffness mechanical metamaterial*. Extreme Mechanics Letters, 2020.
29 **41**: p. 100990.
- 30 13. Wang, Q., et al., *Ultra-low density architected metamaterial with superior mechanical properties and energy*
31 *absorption capability*. Composites Part B: Engineering, 2020. **202**: p. 108379.
- 32 14. Qiu, J., J.H. Lang, and A.H. Slocum, *A curved-beam bistable mechanism*. Journal of Microelectromechanical
33 Systems, 2004. **13**(2): p. 137-146.
- 34 15. Bertoldi, K., et al., *Flexible mechanical metamaterials*. Nature Reviews Materials, 2017. **2**(11): p. 1-11.
- 35 16. Yu, X., et al., *Mechanical metamaterials associated with stiffness, rigidity and compressibility: A brief review*.
36 Progress in Materials Science, 2018. **94**: p. 114-173.
- 37 17. Fu, H., et al., *Morphable 3D mesostructures and microelectronic devices by multistable buckling mechanics*.
38 Nature materials, 2018. **17**(3): p. 268-276.
- 39 18. Hua, J., et al., *A novel design of multistable metastructure with nonuniform cross section*. Journal of Applied
40 Mechanics-Transactions of the Asme, 2022. **89**(5): p. 051010.
- 41 19. Shan, S.C., et al., *Multistable architected materials for trapping elastic strain energy*. Advanced Materials, 2015.

- 1 27(29): p. 4296-4301.
- 2 20. Cherkaev, A., E. Cherkaev, and S. Leelavanichkul. *Principles of optimization of structures against an impact*. in
3 *Journal of Physics: Conference Series*. 2011. IOP Publishing.
- 4 21. Leelavanichkul, S., et al., *Energy absorption of a helicoidal bistable structure*. *Journal of Mechanics of Materials*
5 and *Structures*, 2010. **5**(2): p. 305-321.
- 6 22. Correa, D.M., et al., *Negative stiffness honeycombs for recoverable shock isolation*. *Rapid Prototyping Journal*,
7 2015: p. 193-200.
- 8 23. Restrepo, D., N.D. Mankame, and P.D. Zavattieri, *Phase transforming cellular materials*. *Extreme Mechanics*
9 *Letters*, 2015. **4**: p. 52-60.
- 10 24. Pearson, C.E., *General theory of elastic stability*. *Quarterly of Applied Mathematics*, 1956. **14**(2): p. 133-144.
- 11 25. Timoshenko, S., *Theory of elastic stability 2e*. 1970: Tata McGraw-Hill Education.
- 12 26. Thompson, J., *Basic principles in the general theory of elastic stability*. *Journal of the Mechanics and Physics of*
13 *Solids*, 1963. **11**(1): p. 13-20.
- 14 27. Sobhani, E., et al., *The free vibration analysis of hybrid porous nanocomposite joined hemispherical–cylindrical–*
15 *conical shells*. *Engineering with Computers*, 2021: p. 1-28.
- 16 28. Civalek, Ö., S. Dastjerdi, and B. Akgöz, *Buckling and free vibrations of CNT-reinforced cross-ply laminated*
17 *composite plates*. *Mechanics Based Design of Structures and Machines*, 2022. **50**(6): p. 1914-1931.
- 18 29. Civalek, Ö. and M. Avcar, *Free vibration and buckling analyses of CNT reinforced laminated non-rectangular*
19 *plates by discrete singular convolution method*. *Engineering with Computers*, 2022. **38**(Suppl 1): p. 489-521.
- 20 30. Civalek, Ö., *Geometrically nonlinear dynamic and static analysis of shallow spherical shell resting on two-*
21 *parameters elastic foundations*. *International Journal of Pressure Vessels and Piping*, 2014. **113**: p. 1-9.
- 22 31. Alijani, F. and M. Amabili, *Non-linear vibrations of shells: a literature review from 2003 to 2013*. *International*
23 *Journal of Non-Linear Mechanics*, 2014. **58**: p. 233-257.
- 24 32. Carrera, E., *Theories and finite elements for multilayered plates and shells: a unified compact formulation with*
25 *numerical assessment and benchmarking*. *Archives of Computational Methods in Engineering*, 2003. **10**(3): p.
26 215-296.
- 27 33. Sahu, S.K. and P.K. Datta, *Research advances in the dynamic stability behavior of plates and shells: 1987-2005 -*
28 *Part I: Conservative systems*. *Applied Mechanics Reviews*, 2007. **60**(1-6): p. 65-75.
- 29 34. Moussaoui, F. and R. Benamar, *Non-linear vibrations of shell-type structures: a review with bibliography*. *Journal*
30 *of Sound and Vibration*, 2002. **255**(1): p. 161-184.
- 31 35. Ramm, E., K.-U. Bletzinger, and R. Reitinger, *Shape optimization of shell structures*. *Revue européenne des*
32 *éléments finis*, 1993. **2**(3): p. 377-398.
- 33 36. Stegmann, J. and E. Lund, *Discrete material optimization of general composite shell structures*. *International*
34 *Journal for Numerical Methods in Engineering*, 2005. **62**(14): p. 2009-2027.
- 35 37. Shimoda, M. and Y. Liu, *A non-parametric free-form optimization method for shell structures*. *Structural and*
36 *Multidisciplinary Optimization*, 2014. **50**: p. 409-423.
- 37 38. Sánchez Caballero, S., et al., *Recent advances in structural optimization*. *Annals of The University of Oradea*,
38 2012. **1**(21): p. 118-127.
- 39 39. Zhang, Z., et al., *Bistable morphing composite structures: A review*. *Thin-walled structures*, 2019. **142**: p. 74-97.
- 40 40. Luh, G.-C. and C.-Y. Lin, *Structural topology optimization using ant colony optimization algorithm*. *Applied Soft*
41 *Computing*, 2009. **9**(4): p. 1343-1353.
- 42 41. Perez, R.E. and K. Behdinan, *Particle swarm approach for structural design optimization*. *Computers &*

- 1 Structures, 2007. **85**(19-20): p. 1579-1588.
- 2 42. Wang, M.Y., X.M. Wang, and D.M. Guo, *A level set method for structural topology optimization*. Computer
3 Methods in Applied Mechanics and Engineering, 2003. **192**(1-2): p. 227-246.
- 4 43. Schek, H.-J., *The force density method for form finding and computation of general networks*. Computer methods
5 in applied mechanics and engineering, 1974. **3**(1): p. 115-134.
- 6 44. Xia, L., et al., *Bi-directional evolutionary structural optimization on advanced structures and materials: a
7 comprehensive review*. Archives of Computational Methods in Engineering, 2018. **25**(2): p. 437-478.
- 8 45. Elloumi, W., et al., *The multi-objective hybridization of particle swarm optimization and fuzzy ant colony
9 optimization*. Journal of Intelligent & Fuzzy Systems, 2014. **27**(1): p. 515-525.
- 10 46. Sun, K., et al., *Hybrid ant colony and particle swarm algorithm for solving TSP*. Computer Engineering and
11 Application, 2012. **48**(34): p. 60-63.
- 12 47. Challis, V.J. and J.K. Guest, *Level set topology optimization of fluids in Stokes flow*. International journal for
13 numerical methods in engineering, 2009. **79**(10): p. 1284-1308.
- 14 48. Dühning, M.B., J.S. Jensen, and O. Sigmund, *Acoustic design by topology optimization*. Journal of sound and
15 vibration, 2008. **317**(3-5): p. 557-575.
- 16 49. Rozvany, G.I., *A critical review of established methods of structural topology optimization*. Structural and
17 multidisciplinary optimization, 2009. **37**(3): p. 217-237.
- 18 50. Boutaba, R., et al., *A comprehensive survey on machine learning for networking: evolution, applications and
19 research opportunities*. Journal of Internet Services and Applications, 2018. **9**(1): p. 1-99.
- 20 51. Chowdhury, A., et al., *Image driven machine learning methods for microstructure recognition*. Computational
21 Materials Science, 2016. **123**: p. 176-187.
- 22 52. Deng, L. and X. Li, *Machine learning paradigms for speech recognition: An overview*. IEEE Transactions on
23 Audio, Speech, and Language Processing, 2013. **21**(5): p. 1060-1089.
- 24 53. Erickson, B.J., et al., *Machine learning for medical imaging*. Radiographics, 2017. **37**(2): p. 505-515.
- 25 54. Melville, P. and V. Sindhwani, *Recommender systems*. Encyclopedia of machine learning, 2010. **1**: p. 829-838.
- 26 55. Guo, K., et al., *Artificial intelligence and machine learning in design of mechanical materials*. Materials Horizons,
27 2021. **8**(4): p. 1153-1172.
- 28 56. Wu, L., et al., *A machine learning-based method to design modular metamaterials*. Extreme Mechanics Letters,
29 2020. **36**: p. 100657.
- 30 57. Hanakata, P.Z., et al., *Accelerated search and design of stretchable graphene kirigami using machine learning*.
31 Physical Review Letters, 2018. **121**(25): p. 255304.
- 32 58. Liu, F., et al., *Machine learning-based design and optimization of curved beams for multistable structures and
33 metamaterials*. Extreme Mechanics Letters, 2020. **41**: p. 101002.
- 34 59. Chang, Y., H. Wang, and Q. Dong, *Machine learning-based inverse design of auxetic metamaterial with zero
35 poisson's ratio*. Materials Today Communications, 2022: p. 103186.
- 36 60. Mosavi, A., et al., *Prediction of multi-inputs bubble column reactor using a novel hybrid model of computational
37 fluid dynamics and machine learning*. Engineering Applications of Computational Fluid Mechanics, 2019. **13**(1):
38 p. 482-492.
- 39 61. Xiao, L., et al., *Loading capacity prediction and optimization of cold-formed steel built-up section columns based
40 on machine learning methods*. Thin-Walled Structures, 2022. **180**: p. 109826.
- 41 62. Mangalathu, S. and J.-S. Jeon, *Classification of failure mode and prediction of shear strength for reinforced
42 concrete beam-column joints using machine learning techniques*. Engineering Structures, 2018. **160**: p. 85-94.

- 1 63. Sun, H., H.V. Burton, and H. Huang, *Machine learning applications for building structural design and*
2 *performance assessment: State-of-the-art review*. Journal of Building Engineering, 2021. **33**: p. 101816.
- 3 64. Mai, H.T., J. Kang, and J. Lee, *A machine learning-based surrogate model for optimization of truss structures*
4 *with geometrically nonlinear behavior*. Finite Elements in Analysis and Design, 2021. **196**: p. 103572.
- 5 65. Nashed, M., J. Renno, and M. Mohamed, *Nonlinear analysis of shell structures using image processing and*
6 *machine learning*. Advances in Engineering Software, 2023. **176**: p. 103392.
- 7 66. Keras, A., *Keras API Reference*. Keras Applications. [(accessed on 14 March 2021)].
- 8 67. He, K., et al. *Deep residual learning for image recognition*. in *Proceedings of the IEEE conference on computer*
9 *vision and pattern recognition*. 2016.
- 10 68. Rumelhart, D.E., G.E. Hinton, and R.J. Williams, *Learning representations by back-propagating errors*. nature,
11 1986. **323**(6088): p. 533-536.
- 12 69. Dubey, S.R., S.K. Singh, and B.B. Chaudhuri, *A comprehensive survey and performance analysis of activation*
13 *functions in deep learning*. arXiv preprint arXiv:2109.14545, 2021.
- 14 70. Hoerl, A.E. and R.W. Kennard, *Ridge regression: Biased estimation for nonorthogonal problems*. Technometrics,
15 1970. **12**(1): p. 55-67.
- 16 71. Demir-Kavuk, O., et al., *Prediction using step-wise L1, L2 regularization and feature selection for small data sets*
17 *with large number of features*. BMC Bioinformatics, 2011. **12**.
- 18 72. Chen, J.X., et al., *Fabrication of tough poly (ethylene glycol)/collagen double network hydrogels for tissue*
19 *engineering*. Journal of Biomedical Materials Research Part A, 2018. **106**(1): p. 192-200.
- 20